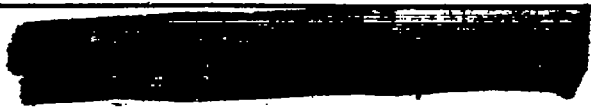


Copy
RM E53F11



TECH LIBRARY KAFB, NM
DL43393

RESEARCH MEMORANDUM

PERFORMANCE COMPARISON OF THREE CANARD-TYPE RAM-JET
MISSILE CONFIGURATIONS AT MACH NUMBERS
FROM 1.5 TO 2.0

By Evan A. Fradenburgh and Emil J. Kremzier

Lewis Flight Propulsion Laboratory
Cleveland, Ohio *Unclassified*

By *NASA Tech Rep Announcement #716*
(OFFICE AUTHORIZED TO CHANGE)

By..... *5 July 57*
K

.....
(GRADE OR OFFICER MAKING CHANGE)
31 Mar 61
DATE

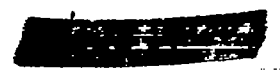
NATIONAL ADVISORY COMMITTEE FOR AERONAUTICS

WASHINGTON
August 14, 1953

RECEIPT SIGNATURE
REQUIRED

NACA RM E53F11

6826





0143393

NACA RM E53F11

NATIONAL ADVISORY COMMITTEE FOR AERONAUTICS

RESEARCH MEMORANDUM

PERFORMANCE COMPARISON OF THREE CANARD-TYPE RAM-JET MISSILE
CONFIGURATIONS AT MACH NUMBERS FROM 1.5 TO 2.0

By Evan A. Fradenburgh and Emil J. Kremzier

SUMMARY

Performance characteristics of three similar canard-type, long-range ram-jet missiles were investigated to evaluate the relative merits of several types of engine installation. Force and engine pressure recovery characteristics of the individual missiles were obtained from previous investigations in the Lewis 8- by 6-foot supersonic wind tunnel at Mach numbers from 1.5 to 2.0 for a range of angle of attack, control surface deflection angle, and engine mass-flow ratio. The engine installations included (1) a twin-engine nacelle-type installation strut-mounted above and below the fuselage in a vertical plane through the fuselage center line, (2) a twin-engine nacelle-type installation mounted on the wing, and (3) a single-engine fuselage-contained installation with an underslung scoop-type inlet. Average Reynolds number based on the mean aerodynamic chord of the wing varied from about 6.9×10^6 to 8.4×10^6 .

Results of the investigation indicated that the lift curve slopes of the three models were about the same and decreased with increasing Mach number. The lowest zero-lift drag was obtained with the underslung scoop-type configuration, probably because of its low projected frontal area. The lowest drag due to lift was measured with the wing-mounted nacelle installation because of the favorable lift interference of the engines. Maximum lift-drag ratio was highest for the underslung scoop-type configuration for most of the Mach number range investigated.

Maximum range of all models increased with Mach number at a given altitude between Mach 1.5 and 2.0 and occurred in the vicinity of critical inlet operation. The underslung scoop-type configuration incorporated a variable-height boundary layer bleed system and usually exhibited a decrease in maximum range with increasing bleed intake height at Mach 2.0 and 50,000 feet altitude because of the relatively high drag of the bleed system. At design Mach number 2.0, the maximum range of all models reached a peak at approximately the design altitude of 50,000 feet. For the design conditions, the longest range was obtained with the underslung scoop-type configuration, although its range was only slightly longer than that of the wing-mounted nacelle-type installation. The shortest range was obtained with the strut-mounted nacelle-type installation.

2931

T-AD

Modification of engine inlets and incorporation of a boundary layer bleed system (where applicable) to improve inlet pressure recoveries were successful in increasing engine efficiencies, but were also associated with rather large increases in drag that resulted in range reductions.

INTRODUCTION

In a missile design, many possibilities exist for the arrangement of the power plant installation. The advantages of one arrangement over another are very difficult to predict because of the complicating effects of aerodynamic interference among the various components of the missile. Nacelle-type air inlets and fuselage-mounted scoop inlets may both be subject to the potential flow field and cross flow separation phenomenon associated with the fuselage and also to the vortex field generated by a forward or canard-type control surface. In addition, the fuselage scoop-type inlet usually requires removal of the fuselage boundary layer ahead of the inlet to obtain efficient inlet operation.

An evaluation of the relative merits of several types of engine installations was made by investigating three similar canard-type missiles having different ram-jet engine installations in the Lewis 8- by 6-foot supersonic wind tunnel to determine their external force and inlet pressure recovery characteristics. Results of the investigations of these missiles are reported separately in references 1 to 3. This report is a summary of the investigations of these missiles in which their external forces, inlet pressure recoveries, and ranges are compared. The engine installations investigated consisted of (1) two nacelle-type engines strut-mounted in a vertical plane through the fuselage center line (ref. 1), (2) two wing-mounted nacelle-type engines (ref. 2), and (3) one fuselage-contained engine with an underslung scoop-type inlet (ref. 3).

The investigations of references 1 to 3 were conducted at Mach numbers of 1.5, 1.8, and 2.0 for a range of angle of attack, canard control surface deflection angle, and engine mass-flow ratio. Range comparisons are presented herein for several initial altitudes in the isothermal region of the atmosphere at each free-stream Mach number. The average test Reynolds numbers based on the mean aerodynamic chord of the wing varied from about 6.9×10^6 to 8.4×10^6 .

SYMBOLS

The following symbols are used in this report:

A duct cross-sectional area

C_D drag coefficient, $\frac{D}{q_0 S}$

| | |
|-----------------------|---|
| C_{D0} | drag coefficient at zero lift |
| C_L | lift coefficient, $\frac{L}{q_0 S}$ |
| C_{T-D} | coefficient of thrust minus drag, $\frac{\text{thrust} - \text{drag}}{q_0 S}$ |
| D | drag |
| $\frac{dC_D}{dC_L^2}$ | drag due to lift |
| f/a | fuel-air ratio |
| H | heating value of fuel, Btu/lb |
| h/R_i | boundary layer scoop height parameter, $\frac{\text{scoop height}}{\text{cowl lip radius}}$ |
| J | mechanical equivalent of heat, 778 ft-lb/Btu |
| L | lift |
| M | Mach number |
| $\frac{m_2}{m_0}$ | engine mass-flow ratio, unity when free-stream tube as defined by cowl lip enters engine |
| P | total pressure |
| p | static pressure |
| q | dynamic pressure, $\frac{\gamma p M^2}{2}$ |
| S | total wing plan-form area |
| V | missile velocity |
| W_f | fuel weight |
| w_f | fuel flow rate |
| W_G | missile gross weight |
| α | missile angle of attack |

2931

CV-1 back

- γ ratio of specific heats
- δ canard control surface deflection angle from body reference line, positive when trailing edge is down
- η_e engine efficiency, $\frac{(\text{thrust}) V}{H J w_f}$
- τ total-temperature ratio across combustion zone

Subscripts:

- 0 free stream
- 2 engine diffuser exit
- max maximum
- t trim, refers to condition of zero pitching moment

DESCRIPTION OF MODELS

The design of the models considered herein was based on an analytical study of long-range ram-jet missiles. A gross weight of 50,000 pounds was selected as representative of this class of aircraft and a flight Mach number of 2.0 was assumed. The study, which included weight estimates of the full-scale components, indicated that the model proportions selected and a design initial altitude of 50,000 feet should be reasonably close to optimum for achieving maximum range for the Mach number and gross weight assumed.

The three canard-type test models (fig. 1) were 1/8 of assumed full scale and had identical wings, control surfaces, and total engine maximum cross-sectional areas. Body volumes were approximately the same. The wing had a plan area of 6.25 square feet, an aspect ratio of 3.0, a taper ratio of 0.5, and a mean aerodynamic chord of 17.97 inches, and the 50 percent chord line was unswept. The airfoil section was a 5 percent thick double circular arc. The all-movable control surface was similar to the wing, with the exception that the thickness was increased to 8 percent near the root for structural reasons. Total control surface plan area was 135 square inches, or 15 percent of the total wing area.

Fuselages of models 1 and 2 (fig. 1) were identical bodies of revolution, pointed at both ends, having a fineness ratio of 12 and a maximum diameter of 9 inches. The engines of model 1 were strut-mounted in a vertical plane through the body center line with their center lines

$1\frac{1}{2}$ engine diameters above and below the body center line. Engine inlets were located at body station 74.1 inches. Because of the limitations imposed by the tunnel support system, model 1 was tested using only one engine, with corrections applied to the data as described in reference 1.

Engine inlets of model 2 were located at body station 54 with their center lines in the plane of the wing, $2\frac{1}{2}$ engine diameters from the fuselage center line. The drags presented for this model in reference 2 were obtained by running two different engines (engine 1 and engine 2) simultaneously. For this analysis, however, it was necessary to obtain drags for two identical engines operating simultaneously. Consequently, the experimental increment of drag due to the engines was weighted in proportion to the theoretical drag attributable to each of the individual engines and the correction was applied to the configuration drag with the engines removed. The estimated effect on lift and pitching moment of operating identical engines in pairs was found to be negligible.

The single-engine underslung scoop-type inlet of model 3 (fig. 1) incorporated a variable-height boundary layer bleed system. The fuselage cross section was approximately circular near the nose and transformed into a flat-bottom section near the semi-circular scoop inlet located at station 55.75 inches. Two separate inlets having 25° and 30° half-conical spikes were investigated on this model, which is described in detail in reference 3.

The vertical fin required for directional stability or control, and shown in figure 1 on models 2 and 3, was not included in the separate investigations of references 2 and 3; consequently it was necessary to correct the drags of these models for the incorporation of the fin. Drag corrections were based on a fin area of 10 percent of the wing area. The engine support struts of model 1 were considered adequate for providing the necessary directional stability for this configuration, thus eliminating the need for a fin drag correction.

As pointed out in references 1, 2, and 3, some small error may be present in the model forces at Mach 1.5 because of tunnel wall shock reflection. In addition, the fairing of the lift curve of model 1 in the higher angle of attack range was somewhat arbitrary for this Mach number because of a lack of experimental data. Whether these possible errors affect the comparison of the model forces at Mach 1.5 is uncertain; consequently the discussion will generally be confined to the higher Mach numbers of 1.8 and 2.0.

Lift and drag data of model 3 presented in reference 3 are uncorrected for tunnel support strut interference because the exact magnitudes of the corrections were unknown. For the present comparison, however,

estimated corrections similar to those applied in references 1 and 2 were applied to the lift and drag data of model 3 and resulted in an angle of zero lift of -0.5° at all free-stream Mach numbers.

RESULTS AND DISCUSSION

External Force and Engine Pressure Recovery Comparison

Configuration lift coefficient for supercritical inlet flow as a function of angle of attack is presented in figure 2 for three models at three free-stream Mach numbers. The lift curve slopes for the three models differ only slightly at a given free-stream Mach number and decrease with increasing Mach number. At Mach numbers of 1.8 and 2.0, the lift curve slope of model 2 is slightly greater than that of the other two models, probably a result arising from the favorable lift interference of the engines (ref. 2). Model 3 has a small amount of lift at zero angle of attack for all Mach numbers because of assymetry of the configuration about the horizontal plane.

Zero-lift drag, drag due to lift, and maximum lift-drag ratio are presented in figure 3 for three models and three free-stream Mach numbers. The lowest zero-lift drag was measured for model 3 (25° inlet, $h/R_1 = 0$), which had the lowest projected frontal area. Of the nacelle-type arrangements, model 1 exhibited the lower zero-lift drag at Mach numbers of 1.8 and 2.0, probably because of the location of the engines in a region of favorable drag interference (ref. 1). This favorable drag interference apparently loses its effectiveness at angle of attack, as evidenced by the fact that the drag due to lift for model 1 is relatively high (also discussed in ref. 1). The lowest drag due to lift was obtained for model 2 and is believed to result from the favorable lift interference of the engines (ref. 2). Model 3 (25° inlet, $h/R_1 = 0$) had the highest maximum lift-drag ratio at M_0 of 1.8 and 2.0, indicating that the effect of its low zero-lift drag on maximum lift-drag ratio outweighed the effect of the low drag due to lift of model 2. Changing engines on model 2 and inlet configuration or boundary layer scoop height on model 3 resulted in a significant change in zero-lift drag, but had a negligible effect on drag due to lift. The effect of these changes on zero-lift drag and maximum lift-drag ratio is shown in the following table:

2931

| Model | $M_0 = 1.5$ | | $M_0 = 1.8$ | | $M_0 = 2.0$ | |
|-----------------------------------|-------------|---------------|-------------|---------------|-------------|---------------|
| | C_{D_0} | $(L/D)_{max}$ | C_{D_0} | $(L/D)_{max}$ | C_{D_0} | $(L/D)_{max}$ |
| 1 | 0.033 | 5.4 | 0.026 | 5.2 | 0.025 | 4.7 |
| 2 (engine 1) | .038 | 5.1 | .032 | 4.9 | .030 | 4.9 |
| 2 (engine 2) | .032 | 5.6 | .029 | 5.2 | .027 | 5.1 |
| 3 (25° inlet $h/R_1 = 0$) | .028 | 5.6 | .024 | 5.7 | .022 | 5.6 |
| 3 (25° inlet $h/R_1 = 0.154$) | .033 | 5.2 | .028 | 5.3 | .025 | 5.3 |
| 3 (30° inlet $h/R_1 = 0$) | .033 | 5.2 | .027 | 5.4 | .024 | 5.4 |
| 3 (30° inlet $h/R_1 = 0.154$) | .038 | 4.8 | .033 | 4.9 | .028 | 5.0 |

Diffuser pressure recovery as a function of mass-flow ratio is presented in figure 4 for three models and three free-stream Mach numbers at zero angle of attack. Pressure recoveries for the three models at Mach 2.0 and 6° angle of attack are also shown. Engine 2 of model 2 was identical to the engines investigated on model 1, and at zero angle of attack has similar pressure recovery characteristics. The data shown in figure 4(d) for a 6° angle of attack are presented to illustrate the effect of angle of attack on engine operation at the design Mach number. All angles of attack of missile operation considered herein lie between 0° and 6°. A detailed discussion of engine mass-flow and pressure recovery characteristics is included in references 1 to 3.

Range Comparison

The assumed full-scale missile range comparison is based on the Breguet range equation with assumptions and method of analysis included in the appendix. Figures 5, 6, and 7 show missile range as a function of diffuser exit Mach number M_2 (which defines engine operating conditions) at three free-stream Mach numbers and several initial altitudes for models 1, 2, and 3, respectively. The maximum range of each configuration at a given altitude and free-stream Mach number occurred in the vicinity of critical inlet operation. Maximum range increased with Mach number at a given altitude for $1.5 \leq M_0 \leq 2.0$.

Variation of range with diffuser exit Mach number M_2 of model 3 at design altitude and Mach number for several boundary layer scoop heights and both inlets is shown in figure 8. The range generally decreased with increasing boundary layer scoop height because of the relatively high drag of the bleed system. A slight increase in range was obtained with the 25° inlet between $h/R_1 = 0$ and $h/R_1 = 0.033$. Some improvement in range is believed to be obtainable through redesign of the boundary layer bleed system. However, range estimates of this model based on known drags of more efficient bleed systems indicate increases in range of only 3 percent over the condition at $h/R_1 = 0$. Apparently the decrease in boundary layer thickness ahead of the inlet for an increase of angle of attack of the underslung scoop-type configuration (see ref. 3) improves the inlet flow conditions to the extent that the value of a boundary layer bleed system may be questionable with respect to range. It should be emphasized that this argument applies only to an underslung scoop-type ram-jet configuration and that further investigation of boundary layer removal systems for other locations of scoop-type inlets is warranted.

The range variation of the three models is summarized in figure 9 where maximum range is presented as a function of initial altitude for the design Mach number of 2.0. The maximum range for all models reaches a peak near design altitude of 50,000 feet. Model 3 exhibits the highest range at all altitudes for both inlets ($h/R_1 = 0$), although it is only slightly higher than model 2. Model 1 has the lowest range at practically all altitudes, and at the design altitude (50,000 ft) its range is considerably below the values calculated for the other two models.

For a given fuel, fuel weight, and gross weight as outlined in the appendix, the engine efficiency η_e and model trim lift-drag ratio $(L/D)_t$ are the two factors in the Breguet range equation that determine range. The greatest range is obtained when the product of these two factors is a maximum. A maximum range comparison and breakdown for the three models investigated is shown in figure 10 for a free-stream Mach number of 2.0 and an altitude of 50,000 feet. The engine efficiency and trim lift-drag ratio of model 1 are somewhat lower than those obtained with the other models, and thus this model has the lowest range. Ranges of models 2 and 3 for the inlets and boundary layer scoop heights investigated are approximately comparable, with model 3 having a slightly greater range for both inlets at $h/R_1 = 0$. The small differences in range between these two models are not considered significant, but it is doubtful whether the range of a configuration such as model 1 could be improved enough, through design modifications, to be considered comparable with models 2 and 3.

The pressure recovery of engine 1 of model 2 was higher than that of engine 2, and a higher engine efficiency η_e for engine 1 resulted (fig. 10). This higher pressure recovery was accompanied by an increase

in drag, however, and the $(L/D)_t$ of the configuration was reduced. The resulting range obtained with engine 1 was less than that obtained with engine 2, indicating that the beneficial effects of the increased pressure recovery on η_e were outweighed by the detrimental effects of the increase in drag on $(L/D)_t$. A similar situation exists between the 25° and 30° inlets of model 3 (fig. 10). For $h/R_1 = 0.154$, the effects of the higher drag of the 30° inlet on $(L/D)_t$ outweighed the effects of the higher pressure recovery on η_e with a resulting decrease in range. At $h/R_1 = 0$, the effects of the increased drag of the 30° inlet on $(L/D)_t$ are just balanced by the effects of the increased pressure recovery on η_e , and the range is unchanged. As discussed previously, both inlets of model 3 exhibited a reduction in range for an increase of boundary layer scoop height from $h/R_1 = 0$ to $h/R_1 = 0.154$ because of the detrimental effects of the relatively high bleed system drag on $(L/D)_t$.

Excess Thrust

Aside from the problem of long-range operation, the missile flight plan may include a short period of acceleration, climb, or maneuvering. A detailed analysis of these factors is beyond the scope of this report; however, a brief presentation of the excess thrust available for acceleration, climb, or maneuvering is included in figure 11. Maximum C_{T-D} is presented as a function of C_{L_t} at three free-stream Mach numbers for models 1, 2, and 3. Maximum C_{T-D} occurs in the vicinity of critical inlet operation and, for a given M_2 , is obtained by increasing the fuel flow and nozzle size until straight pipe choking or maximum τ available from the fuel is reached, whichever occurs first. The values of C_{L_t} required for various operating altitudes at the Mach numbers presented are indicated in the figure. The maximum altitude at which level flight can be maintained is reached when maximum C_{T-D} available becomes zero.

Maximum C_{T-D} for both engines of model 2 is presented in figure 11(b). Engine 1 has the higher maximum C_{T-D} at Mach 2.0 because of its higher pressure recovery. At Mach 1.5 and 1.8, maximum C_{T-D} of engine 1 is lower than that of engine 2 because its superiority in pressure recovery is very slight or even negligible, while its drag remains relatively high.

For model 3 (fig. 11(c)), the maximum C_{T-D} for the 25° inlet usually increases as h/R_1 is increased from 0 to 0.154. This margin of increase becomes smaller at the higher values of C_{L_t} because the

improvement in engine pressure recovery with increasing h/R_1 drops off at the higher angles of attack (ref. 3) and the drag increase becomes more significant. For the 30° inlet, however, an increase in h/R_1 from 0 to 0.154 results in a decrease of maximum C_{T-D} at Mach numbers of 1.5 and 1.8. The pressure recovery increase for this case is relatively small and at the higher angles of attack actually decreases with an increase in h/R_1 (ref. 3). At Mach 2.0, the maximum C_{T-D} is approximately the same for $h/R_1 = 0$ and $h/R_1 = 0.154$ because the margin of increase of pressure recovery is somewhat greater than that for Mach 1.5 and 1.8 and just balances the drag increase. A lower drag boundary layer removal system would, of course, result in an increase of maximum C_{T-D} with an increase in h/R_1 for this case.

If the ram-jet engines are used to furnish part of the boost to design Mach number and altitude for these missiles, a reduction in range will be realized. By employing a variable-size exit nozzle that reexpands to combustion chamber diameter, it is possible to obtain a boost flight path at maximum C_{T-D} that includes acceleration from Mach 1.5 to 2.0 at 35,332 feet altitude and climb from 35,332 feet to 50,000 feet altitude at Mach 2.0. The remainder of the flight would then follow the Breguet flight path at cruise conditions. An estimate of the reduction in range obtained with models 1, 2 (engine 2), and 3 (25° inlet, $h/R_1 = 0$) for this flight path was made, and an approximate 5 percent reduction in range from that obtained for the design flight path (external boost to design Mach number and altitude) was calculated.

SUMMARY OF RESULTS

An analysis of the performance characteristics of three canard-type, long-range ram-jet missiles determined from the results of previous investigations is presented for Mach numbers from 1.5 to 2.0. The investigation covered a range of angle of attack, control surface deflection angle, and engine mass-flow ratio. The missile configurations were similar except for their engine installations which included (1) a twin-engine nacelle-type installation strut-mounted above and below the fuselage in a vertical plane through the fuselage center line, (2) a twin-engine nacelle-type installation mounted on the wing on either side of the fuselage, and (3) a single fuselage-contained engine with an under-slung scoop-type inlet. The following results were obtained:

1. The lift curve slopes for the three models were about the same and decreased with increasing Mach number. At Mach numbers of 1.8 and 2.0, the lift curve slope of model 2 was slightly greater than that for the other two models, probably because of the favorable lift interference of the engines.

2. The lowest zero-lift drag was obtained with model 3 (25° inlet, boundary layer scoop height parameter of 0), probably because of its low projected frontal area. Model 2 (engine 2) had the lowest drag due to lift because of the favorable lift interference of the engines. Model 3 (25° inlet, boundary layer scoop height parameter of 0) exhibited the highest maximum lift-drag ratio for most of the Mach number range investigated.

3. Maximum range of all models increased with Mach number at a given altitude for the Mach number range investigated and occurred in the vicinity of critical inlet operation.

4. For model 3 at Mach 2.0 and 50,000 feet altitude, the maximum range usually decreased with increasing boundary layer scoop height as a result of the relatively high drag of the boundary layer bleed system. Range estimates for this model based on known drags of more efficient bleed systems indicate that only slight increases in range are obtainable, however.

5. At Mach 2.0, the maximum range of all models reached a peak at approximately the design altitude of 50,000 feet. The longest range was obtained with model 3, although it was only slightly longer than that of model 2. Model 1 had the shortest range at practically all altitudes.

6. Relatively high engine efficiencies were attained through boundary layer removal and design of inlets for high pressure recoveries, but the drag penalties associated with the particular designs considered herein generally resulted in a reduction in maximum range from that obtained for the lower drag configurations with only moderately high pressure recoveries.

Lewis Flight Propulsion Laboratory
National Advisory Committee for Aeronautics
Cleveland, Ohio, May 21, 1953

2931

CV-2 back

APPENDIX - ASSUMPTIONS AND METHOD OF ANALYSIS

For the range calculations, the full-scale models were assumed to operate at constant C_{L_t} in the isothermal region of the atmosphere (35,332 ft to 105,000 ft altitude). With the minor changes in missile drag coefficient due to variations in Reynolds number neglected, $(L/D)_t$ remains constant for a given C_{L_t} and M_2 and the engines operate at a constant thrust coefficient. If the missile flight velocity and engine combustion efficiency are assumed constant, η_e is constant. Under these conditions, the altitude of the missile gradually increases as fuel is consumed and the following form of the Breguet range equation applies:

$$\text{Range} = HJ \eta_e (L/D)_t \ln \left(\frac{W_G}{W_G - W_f} \right) \quad \text{feet} \quad (1)$$

Values assumed for the factors in this equation that are independent of missile operating conditions are as follows:

$H = 19,170$ Btu/lb (typical hydrocarbon fuel of composition $(CH_2)_x$)

$W_G = 50,000$ lb

$W_f = 30,000$ lb

Differences in missile structural weight arising from the variations in power plant installation may influence the relative comparison of missile ranges, but are beyond the scope of this report and have not been considered. Values of $(L/D)_t$ for the individual missiles were obtained from an interpolation of the curves in references 1 to 3 for the particular conditions of missile operation required. Drags due to control surface deflections required for trim produced only minor changes in missile lift-drag ratios. The effect of the differences between individual missile trim drags on the relative comparison of missile ranges was therefore considered negligible. Lift coefficients required for level flight were calculated from the assumed full-scale missile wing area of 400 square feet. Engine efficiency η_e was determined for thrust coefficient equal to the drag coefficient. Required thrust was obtained by balancing the heat addition and nozzle size for the assumed combustion chamber Mach number using the energy, momentum, and continuity equations. A convergent-divergent nozzle reexpanding to maximum combustion chamber diameter was employed. The following assumptions were made with regard to the heat addition process:

Heat added in constant-area channel

Total-pressure loss across fuel spray and flame holder = $2q_2$

γ before combustion = 1.4

γ after combustion = 1.3

γ through nozzle reexpansion = 1.34

Total-pressure ratio across nozzle = 0.98

Fuel-air ratio was determined from a set of curves of flame temperature as a function of fuel-air ratio for various initial temperatures such as those presented in reference 4, assuming a combustion efficiency of 100 percent.

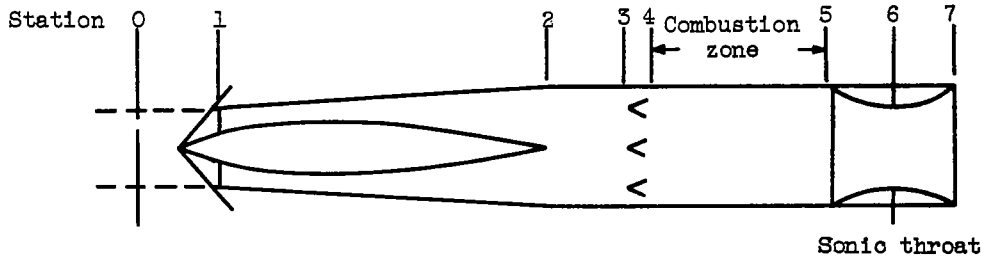
Conditions of missile and engine operation for several values of combustion chamber Mach number are presented in table I for the design Mach number and altitude. Representative values of τ , f/a , and A_5/A_6 are shown in the table. Off-design operating conditions for model 2 (engine 2) are presented in table II for values of M_2 at which maximum range occurs.

REFERENCES

1. Obery, Leonard J., and Krasnow, Howard S.: Performance Characteristics of Canard-Type Missile with Vertically Mounted Nacelle Engines at Mach Numbers 1.5 to 2.0. NACA RM E52H08, 1952.
2. Kremzier, Emil J., and Davids, Joseph: Performance Characteristics of Canard-Type Missile with Wing-Mounted Nacelle Engines at Mach Numbers 1.5 to 2.0. NACA RM E52J08, 1952.
3. Fradenburgh, Evan A., and Campbell, Robert C.: Characteristics of a Canard-Type Missile Configuration with an Underslung Scoop Inlet at Mach Numbers from 1.5 to 2.0. NACA RM E52J22, 1953.
4. Williams, Glenn C., and Quinn, John C.: Ram Jet Power Plants. Jet Propelled Missiles Panel, OSRD, May 1945. (Under Assignment to Coordinator of Research and Development, U. S. Navy.)

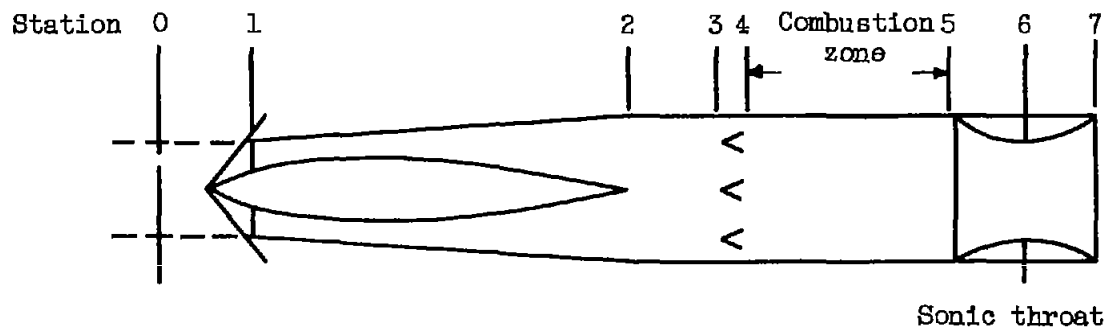
TABLE I. - MISSILE DESIGN OPERATING CONDITIONS

$$[M_0 = 2.0; \text{altitude} = 50,000 \text{ ft}; C_{L_t} = 0.1843]$$

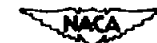


| Model | M_2 | α , deg | δ , deg | C_D | $(L/D)_t$ | m_2/m_0 | P_2/P_0 | τ | f/a | A_5/A_6 | η_e | Range, miles |
|---|-------|----------------|----------------|--------|-----------|-----------|-----------|--------|--------|-----------|----------|--------------|
| 1 | 0.14 | 3.70 | 2.52 | 0.0487 | 3.784 | 0.822 | 0.799 | 5.25 | 0.0503 | 1.616 | 0.178 | 1745 |
| | .15 | | | .0468 | 3.938 | .880 | .798 | 4.77 | .0431 | 1.574 | .187 | 1902 |
| | .16 | | | .0452 | 4.077 | .927 | .788 | 4.44 | .0386 | 1.519 | .191 | 2016 |
| | .17 | | | .0441 | 4.179 | .962 | .771 | 4.26 | .0361 | 1.447 | .192 | 2077 |
| | .18 | | | .0438 | 4.208 | .968 | .734 | 4.31 | .0367 | 1.332 | .186 | 2051 |
| 2 Engine 1 | 0.14 | 3.38 | 0.64 | 0.0426 | 4.326 | 0.830 | 0.883 | 3.99 | 0.0326 | 1.903 | 0.217 | 2432 |
| | .15 | | | .0416 | 4.430 | .869 | .868 | 3.75 | .0295 | 1.821 | .224 | 2568 |
| | .16 | | | .0413 | 4.462 | .884 | .828 | 3.78 | .0299 | 1.679 | .216 | 2491 |
| | .17 | | | .0413 | 4.462 | .884 | .782 | 3.87 | .0311 | 1.534 | .207 | 2396 |
| | .18 | | | .0413 | 4.462 | .884 | .739 | 3.99 | .0326 | 1.399 | .198 | 2288 |
| 2 Engine 2 | 0.14 | 3.38 | 0.64 | 0.0427 | 4.316 | 0.838 | 0.825 | 4.35 | 0.0374 | 1.807 | 0.206 | 2303 |
| | .15 | | | .0395 | 4.666 | .894 | .814 | 3.94 | .0319 | 1.768 | .209 | 2531 |
| | .16 | | | .0384 | 4.799 | .931 | .794 | 3.74 | .0294 | 1.687 | .212 | 2636 |
| | .17 | | | .0379 | 4.863 | .950 | .769 | 3.68 | .0286 | 1.583 | .211 | 2657 |
| | .18 | | | .0376 | 4.902 | .965 | .735 | 3.71 | .0290 | 1.467 | .203 | 2579 |
| 3 25° inlet $\frac{h}{R_1} = 0$ | 0.17 | 3.16 | 1.78 | 0.0359 | 5.134 | 0.848 | 0.688 | 3.97 | 0.0323 | 1.511 | 0.195 | 2587 |
| | .18 | | | .0347 | 5.311 | .893 | .685 | 3.68 | .0286 | 1.474 | .202 | 2775 |
| | .19 | | | .0342 | 5.389 | .911 | .665 | 3.64 | .0281 | 1.384 | .198 | 2768 |
| | .20 | | | .0341 | 5.405 | .916 | .636 | 3.75 | .0295 | 1.266 | .187 | 2624 |
| | .21 | | | .0340 | 5.421 | .918 | .608 | 3.97 | .0323 | 1.137 | .170 | 2390 |
| 3 25° inlet $\frac{h}{R_1} = 0.154$ | 0.14 | 3.16 | 1.78 | 0.0445 | 4.142 | 0.787 | 0.771 | 4.88 | 0.0447 | 1.691 | 0.188 | 2015 |
| | .15 | | | .0427 | 4.316 | .838 | .767 | 4.46 | .0387 | 1.641 | .196 | 2186 |
| | .16 | | | .0409 | 4.506 | .887 | .763 | 4.07 | .0336 | 1.607 | .204 | 2378 |
| | .17 | | | .0395 | 4.666 | .928 | .756 | 3.74 | .0294 | 1.570 | .215 | 2598 |
| | .18 | | | .0385 | 4.787 | .957 | .735 | 3.64 | .0281 | 1.482 | .213 | 2636 |
| | .19 | | | .0381 | 4.837 | .967 | .704 | 3.70 | .0289 | 1.370 | .202 | 2536 |
| 3 30° inlet $\frac{h}{R_1} = 0$ | 0.15 | 3.16 | 1.78 | 0.0359 | 5.134 | 0.851 | 0.755 | 3.78 | 0.0299 | 1.738 | 0.209 | 2786 |
| | .16 | | | .0359 | 5.134 | .853 | .734 | 3.83 | .0305 | 1.661 | .205 | 2724 |
| | .17 | | | .0358 | 5.148 | .855 | .696 | 3.88 | .0311 | 1.531 | .200 | 2665 |
| | .18 | | | .0358 | 5.148 | .855 | .657 | 4.01 | .0329 | 1.397 | .189 | 2519 |
| 3 30° inlet $\frac{h}{R_1} = 0.154$ | 0.14 | 3.16 | 1.78 | 0.0423 | 4.357 | 0.849 | 0.834 | 4.11 | 0.0341 | 1.874 | 0.217 | 2448 |
| | .15 | | | .0413 | 4.462 | .877 | .808 | 3.96 | .0322 | 1.764 | .217 | 2509 |
| | .16 | | | .0410 | 4.495 | .886 | .763 | 4.07 | .0337 | 1.607 | .204 | 2374 |
| | .17 | | | .0409 | 4.506 | .889 | .725 | 4.12 | .0343 | 1.477 | .199 | 2324 |
| | .18 | | | .0408 | 4.517 | .892 | .685 | 4.21 | .0362 | 1.342 | .188 | 2194 |

TABLE II. - MISSILE OFF-DESIGN OPERATING CONDITIONS (MODEL 2, ENGINE 2)



| M_0 | Altitude, ft | C_{I_t} | α , deg | δ , deg | M_2 | C_D | $(L/D)_t$ | m_2/m_0 | P_2/P_0 | τ | f/a | A_5/A_6 | η_e | Range, miles |
|-------|--------------|-----------|----------------|----------------|-------|--------|-----------|-----------|-----------|--------|--------|-----------|----------|--------------|
| 1.5 | 35,332 | 0.1621 | 2.34 | 0.57 | 0.17 | 0.0383 | 4.232 | 0.811 | 0.939 | 4.54 | 0.0302 | 1.390 | 0.1326 | 1453 |
| | 40,000 | .2026 | 2.91 | .77 | .17 | .0420 | 4.824 | .812 | .940 | 4.92 | .0340 | 1.317 | .1293 | 1615 |
| 1.8 | 35,332 | 0.1125 | 1.95 | 0.44 | 0.17 | 0.0321 | 3.505 | 0.899 | 0.851 | 3.40 | 0.0226 | 1.665 | 0.1930 | 1753 |
| | 40,000 | .1407 | 2.42 | .55 | .17 | .0343 | 4.102 | .897 | .849 | 3.58 | .0247 | 1.616 | .1891 | 2009 |
| | 50,000 | .2275 | 3.77 | .88 | .16 | .0439 | 5.182 | .873 | .873 | 4.54 | .0355 | 1.500 | .1735 | 2328 |
| 2.0 | 35,332 | 0.0911 | 1.67 | 0.26 | 0.17 | 0.0305 | 2.987 | 0.963 | 0.779 | 3.05 | 0.0210 | 1.782 | 0.2275 | 1760 |
| | 40,000 | .1140 | 2.09 | .35 | .17 | .0318 | 3.585 | .960 | .777 | 3.15 | .0222 | 1.743 | .2250 | 2090 |
| | 50,000 | .1843 | 3.38 | .64 | .17 | .0379 | 4.863 | .950 | .769 | 3.68 | .0286 | 1.580 | .2109 | 2657 |
| | 60,000 | .2959 | 5.39 | 1.28 | .17 | .0555 | 5.332 | .929 | .752 | 5.66 | .0581 | 1.198 | .1556 | 2149 |



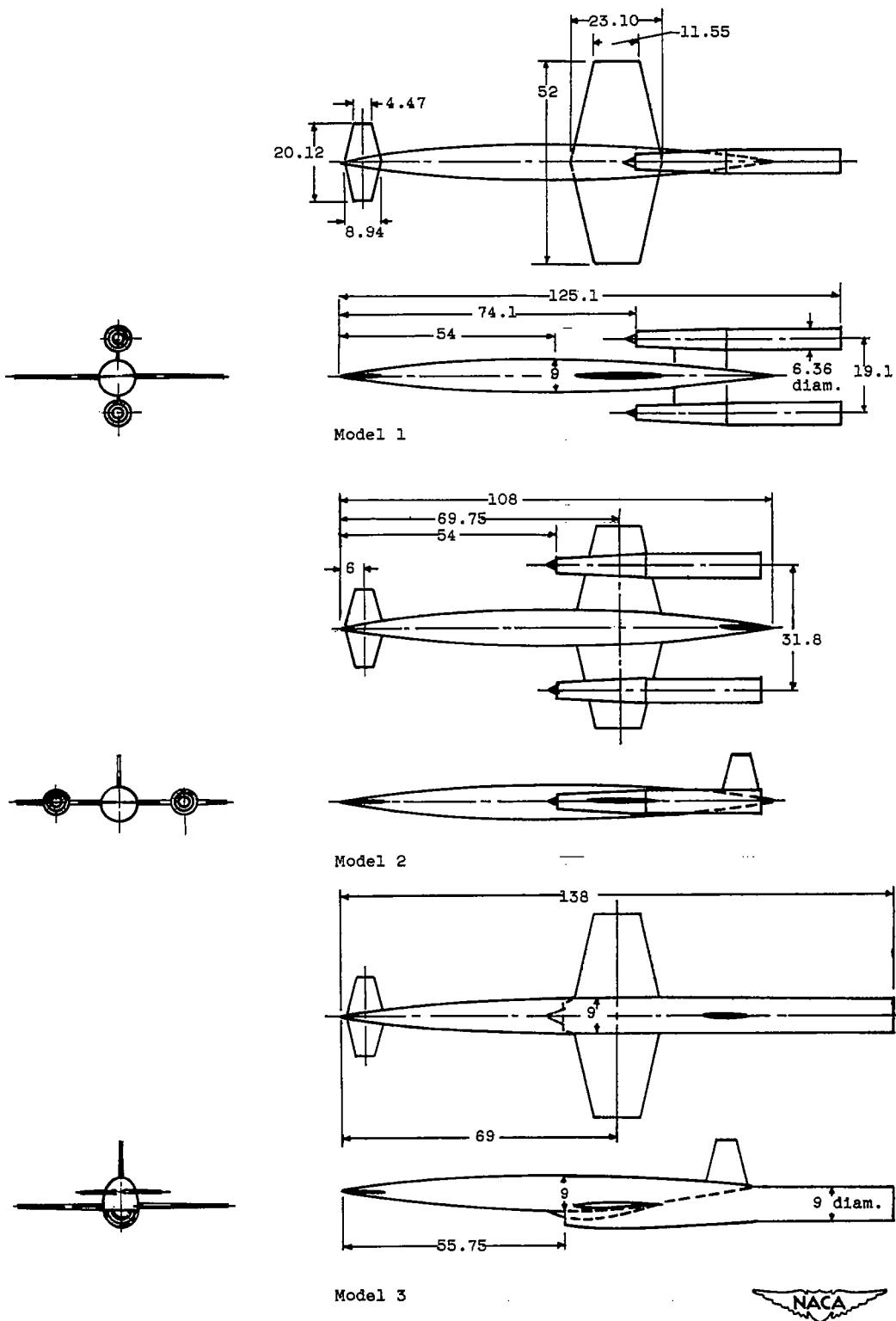


Figure 1. - Sketch of models. (All dimensions are in inches.)

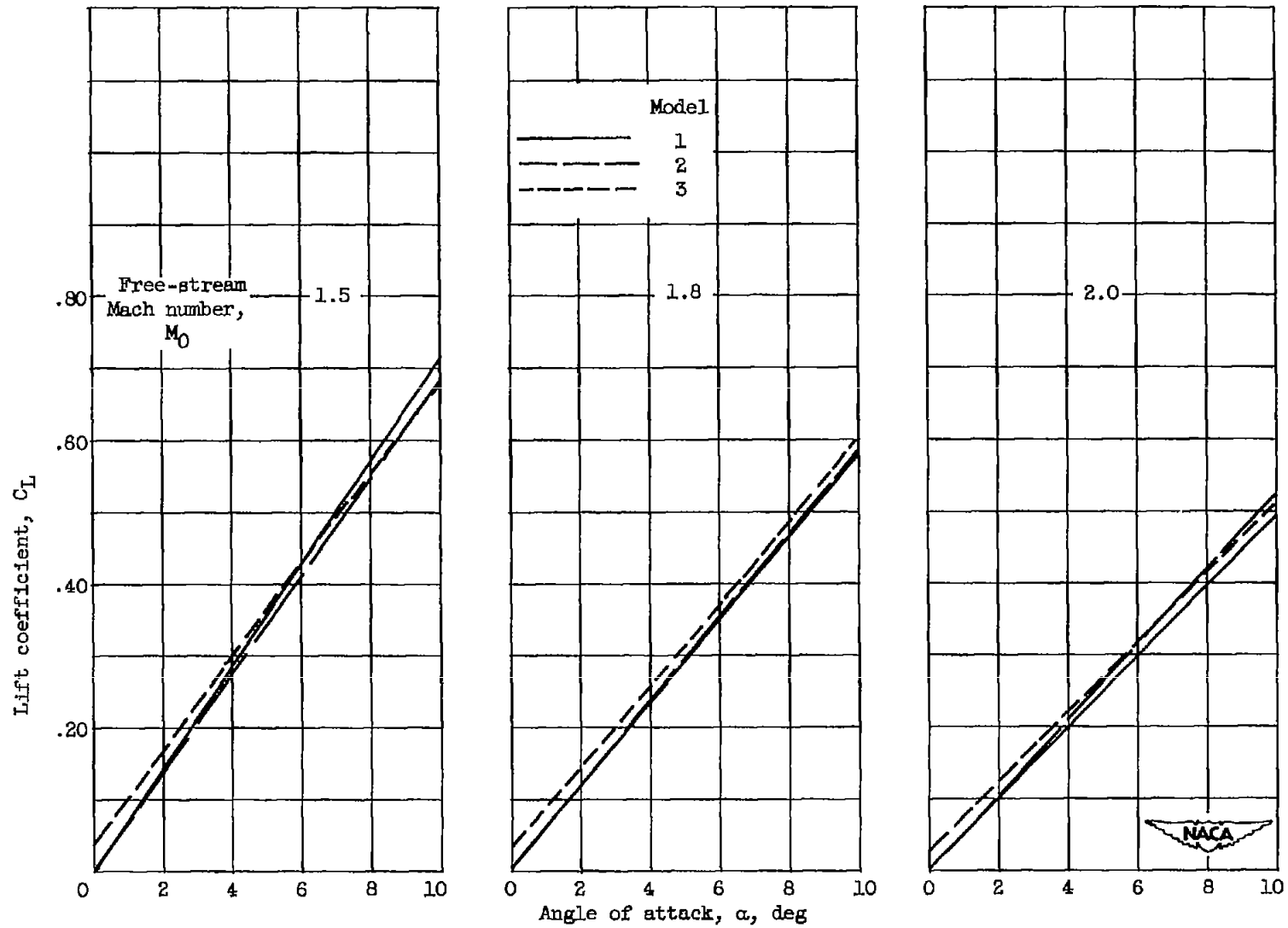


Figure 2. - Variation of configuration lift coefficient with angle of attack for three models and three Mach numbers. $\delta, 0^\circ$ (supercritical inlet operation).

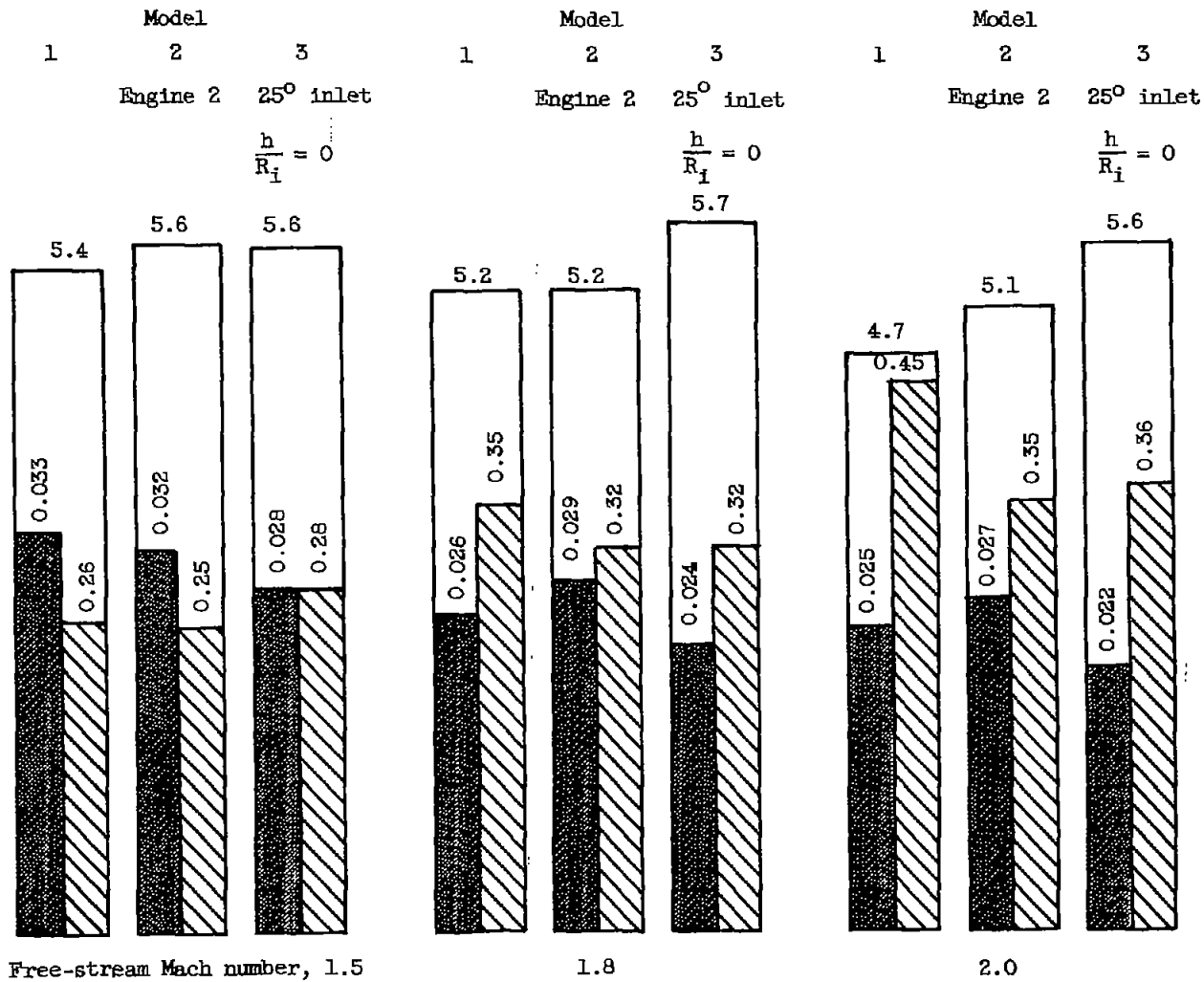
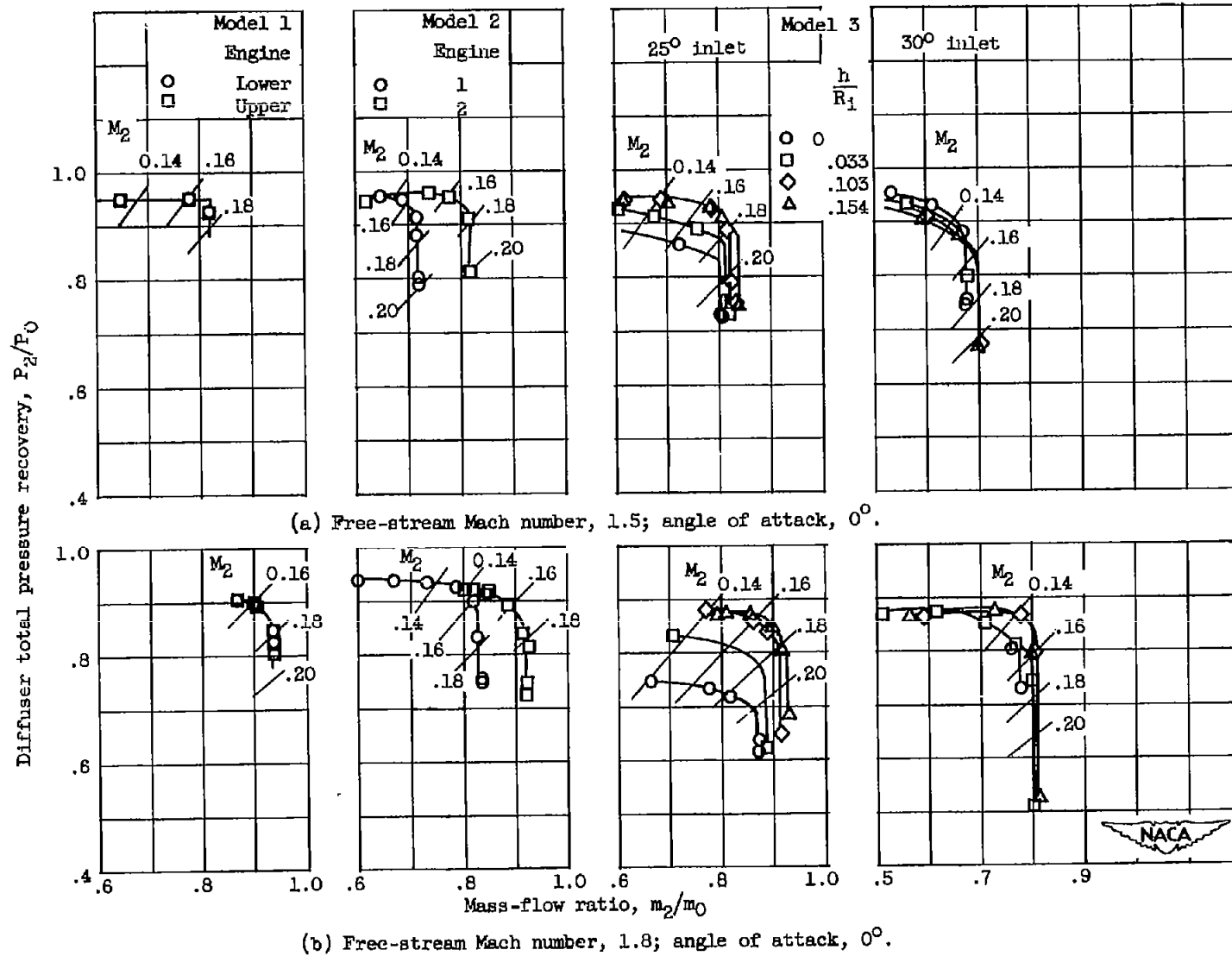


Figure 3. - Comparison of zero-lift drag, drag due to lift, and maximum lift-drag ratio for three models and three free-stream Mach numbers. $\delta, 0^\circ$ (supercritical inlet operation).

Figure 4. - Variation of total pressure recovery with mass-flow ratio. $5, 0^\circ$.

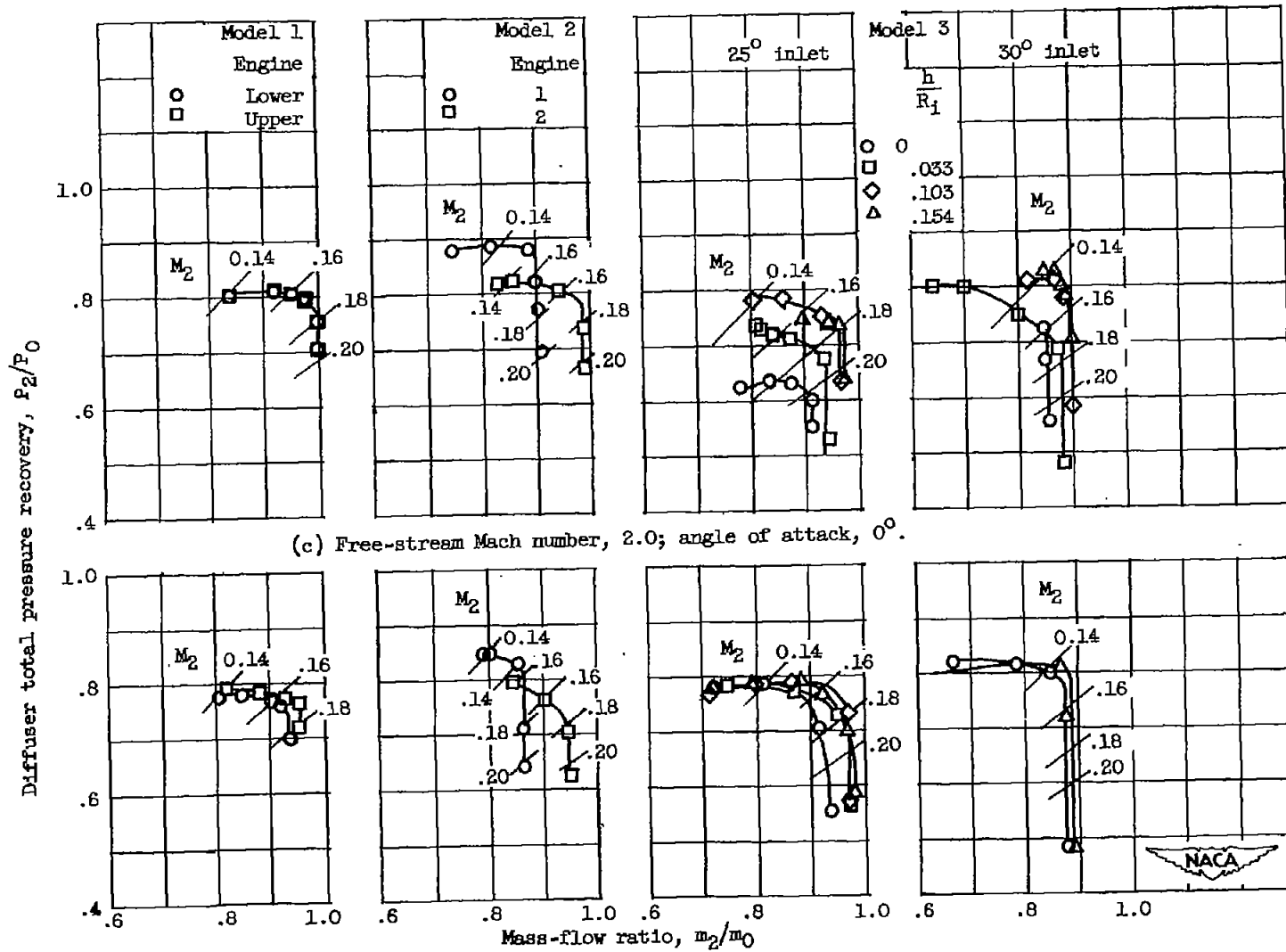


Figure 4. - Concluded. Variation of total pressure recovery with mass-flow ratio. 8, 0° .

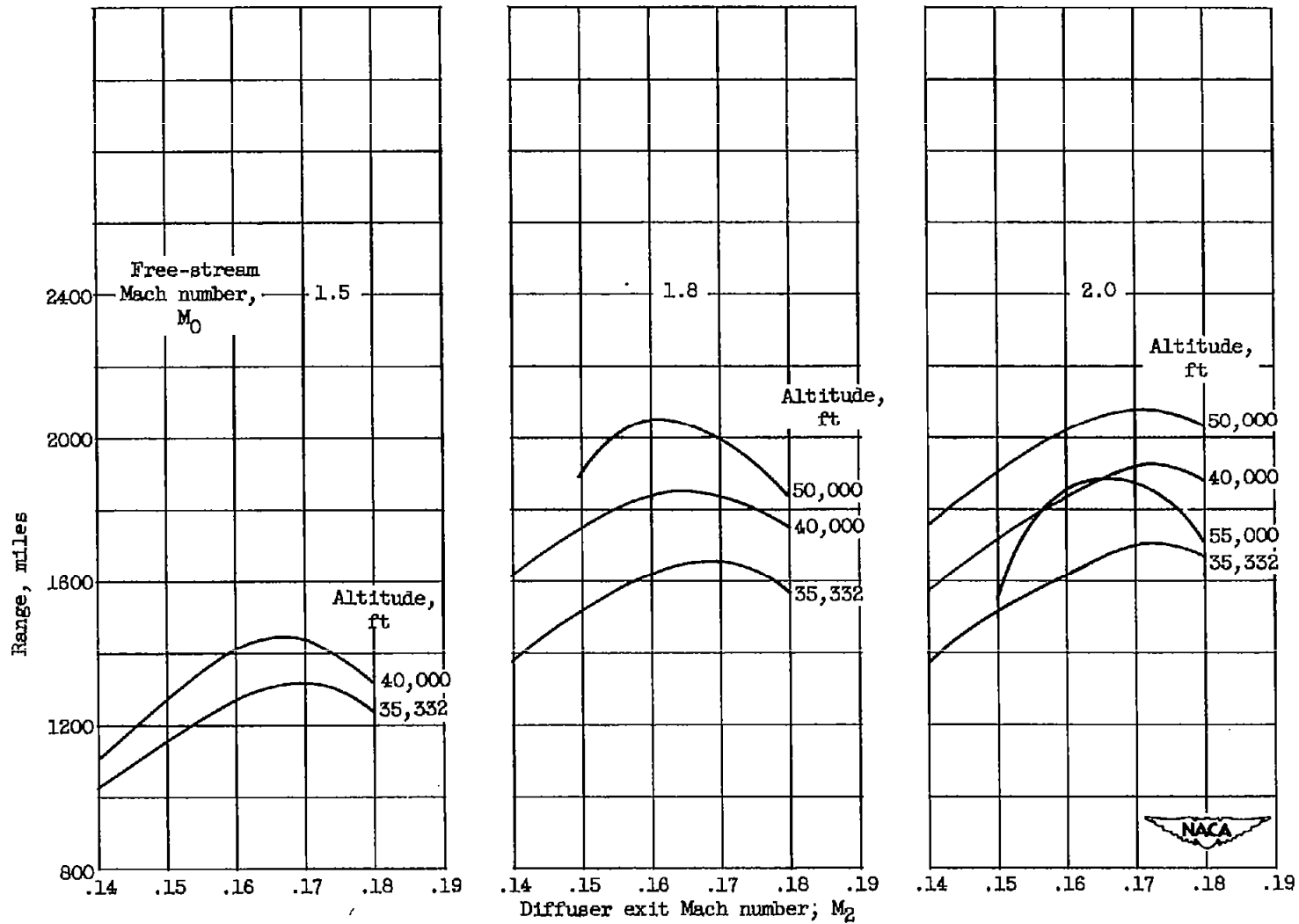
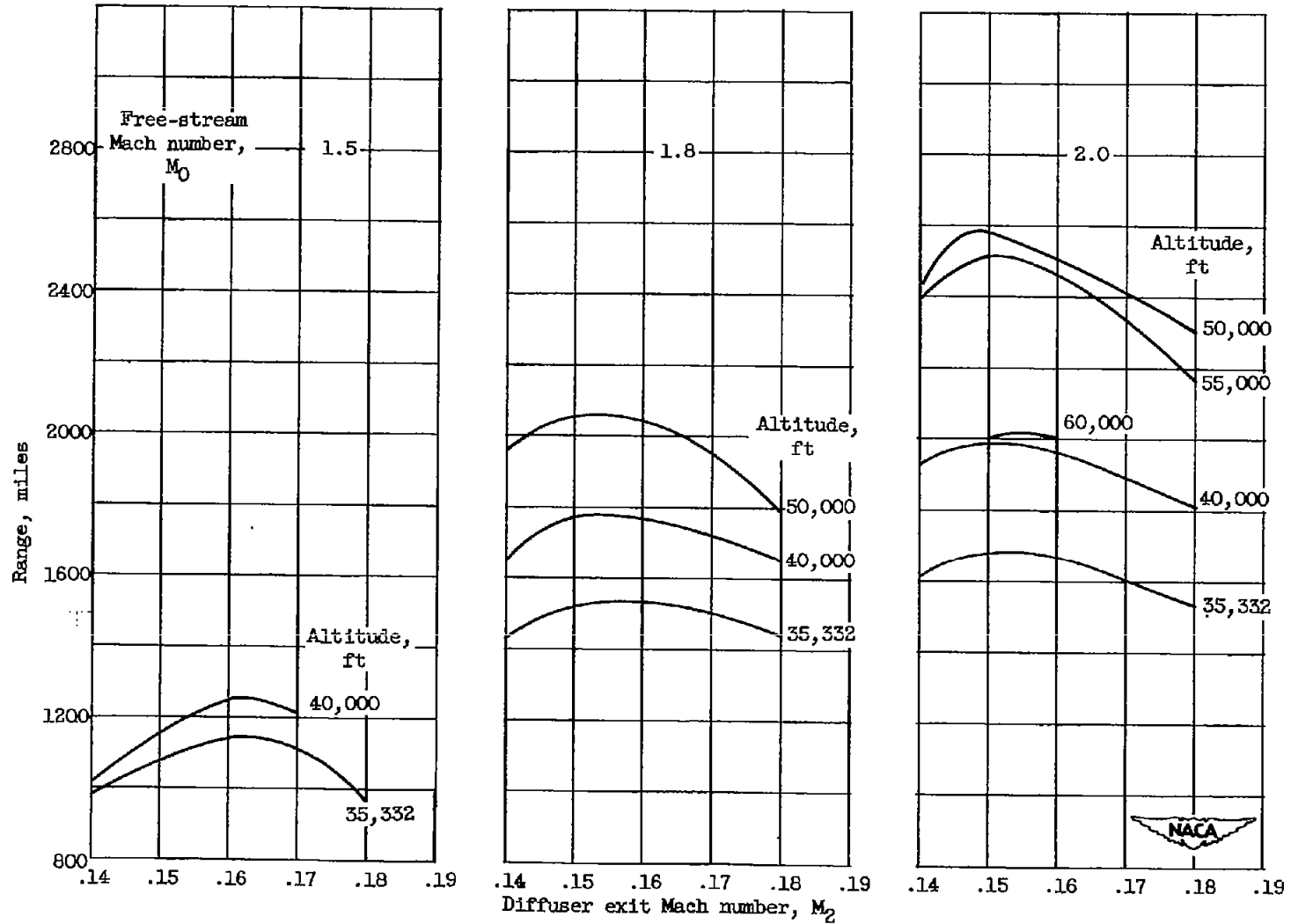
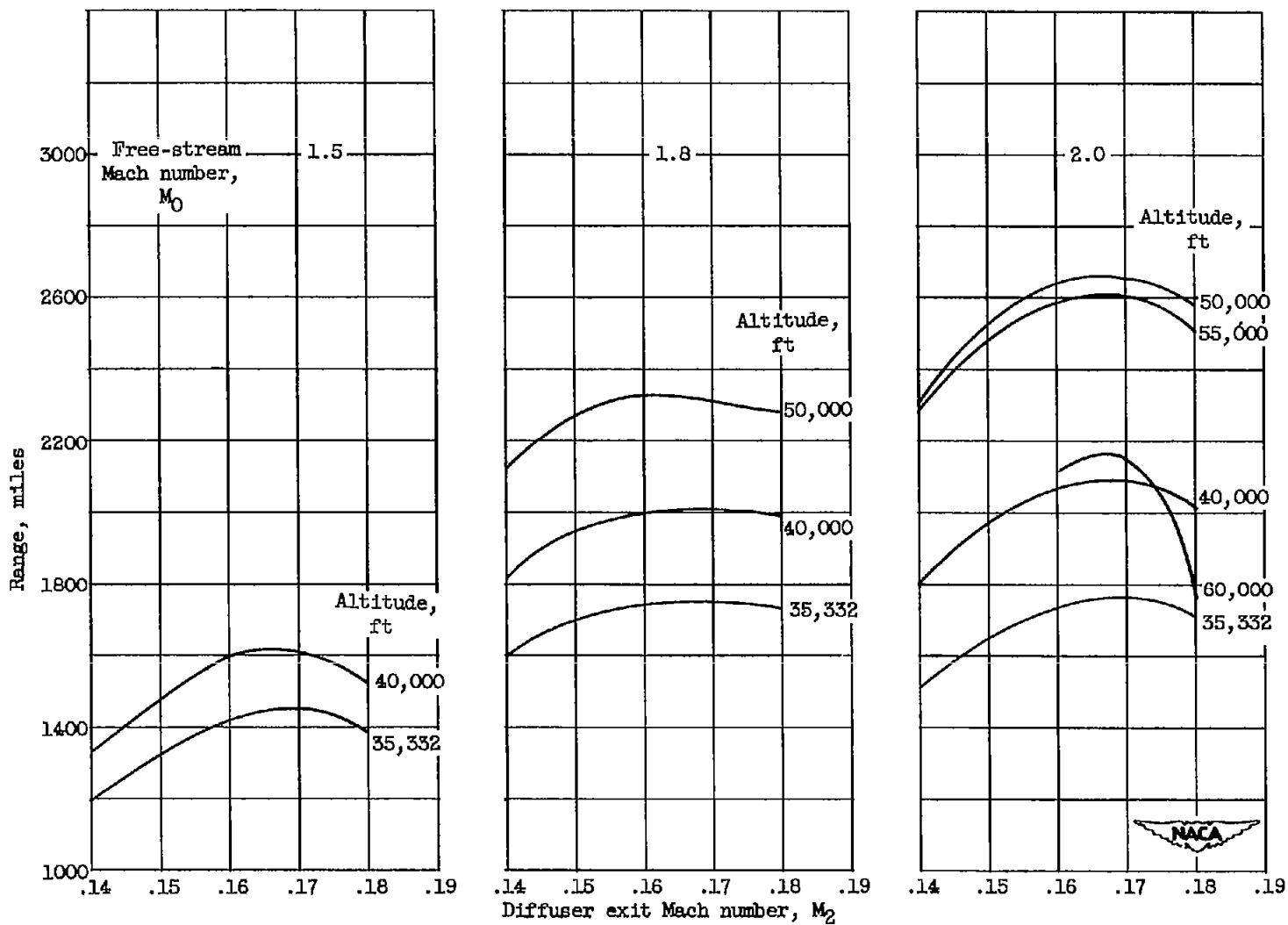


Figure 5. - Variation of range with diffuser exit Mach number for model 1 at three free-stream Mach numbers and several altitudes.



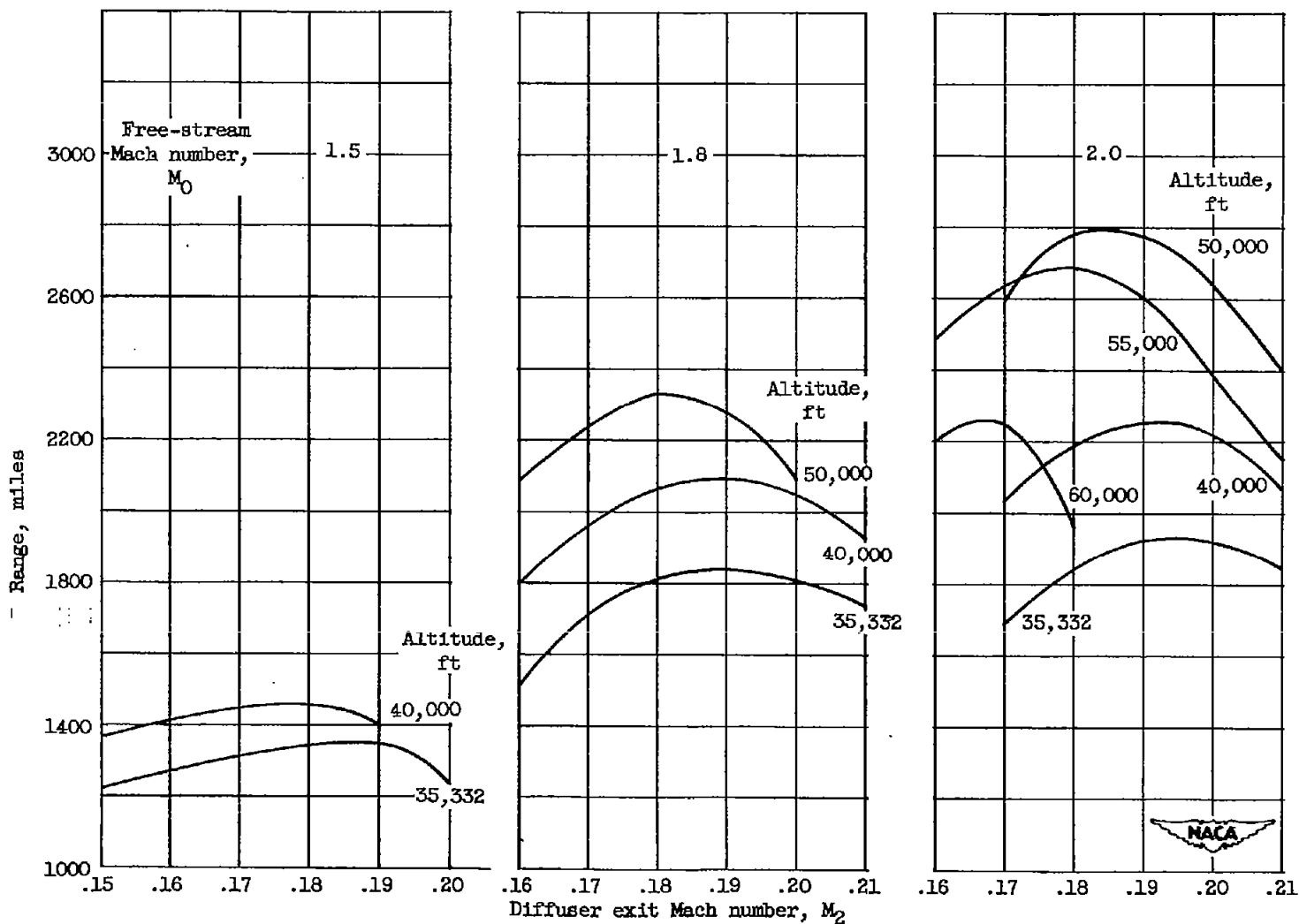
(a) Engine 1.

Figure 6. - Variation of range with diffuser exit Mach number for model 2 at three free-stream Mach numbers and several altitudes.



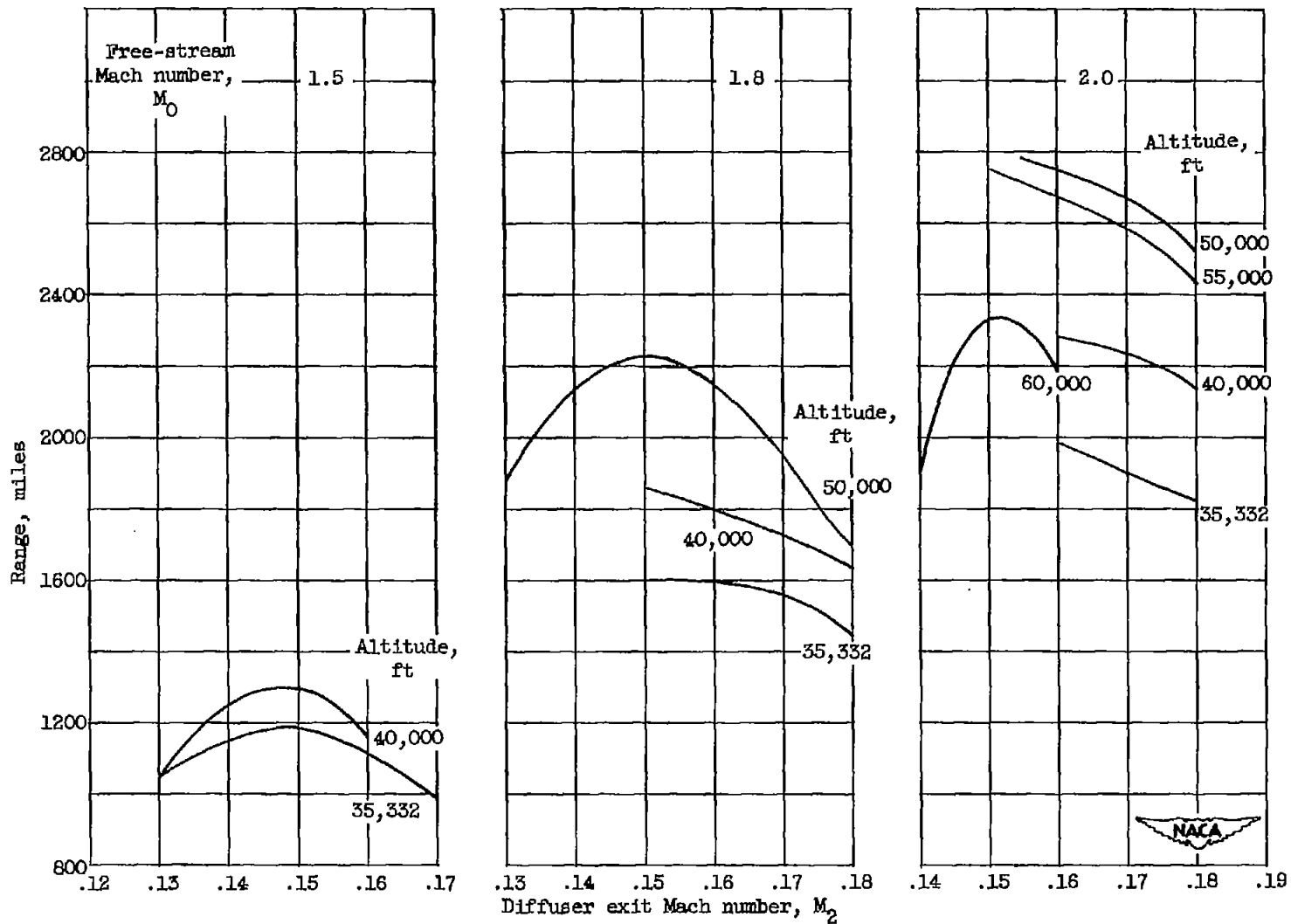
(b) Engine 2.

Figure 6. - Concluded. Variation of range with diffuser exit Mach number for model 2 at three free-stream Mach numbers and several altitudes.



(a) 25° inlet; boundary layer scoop height parameter, 0.

Figure 7. - Variation of range with diffuser exit Mach number for model 3 at three free-stream Mach numbers and several altitudes.



(b) 30° inlet; boundary layer scoop height parameter, 0.

Figure 7. - Concluded. Variation of range with diffuser exit Mach number for model 3 at three free-stream Mach numbers and several altitudes.

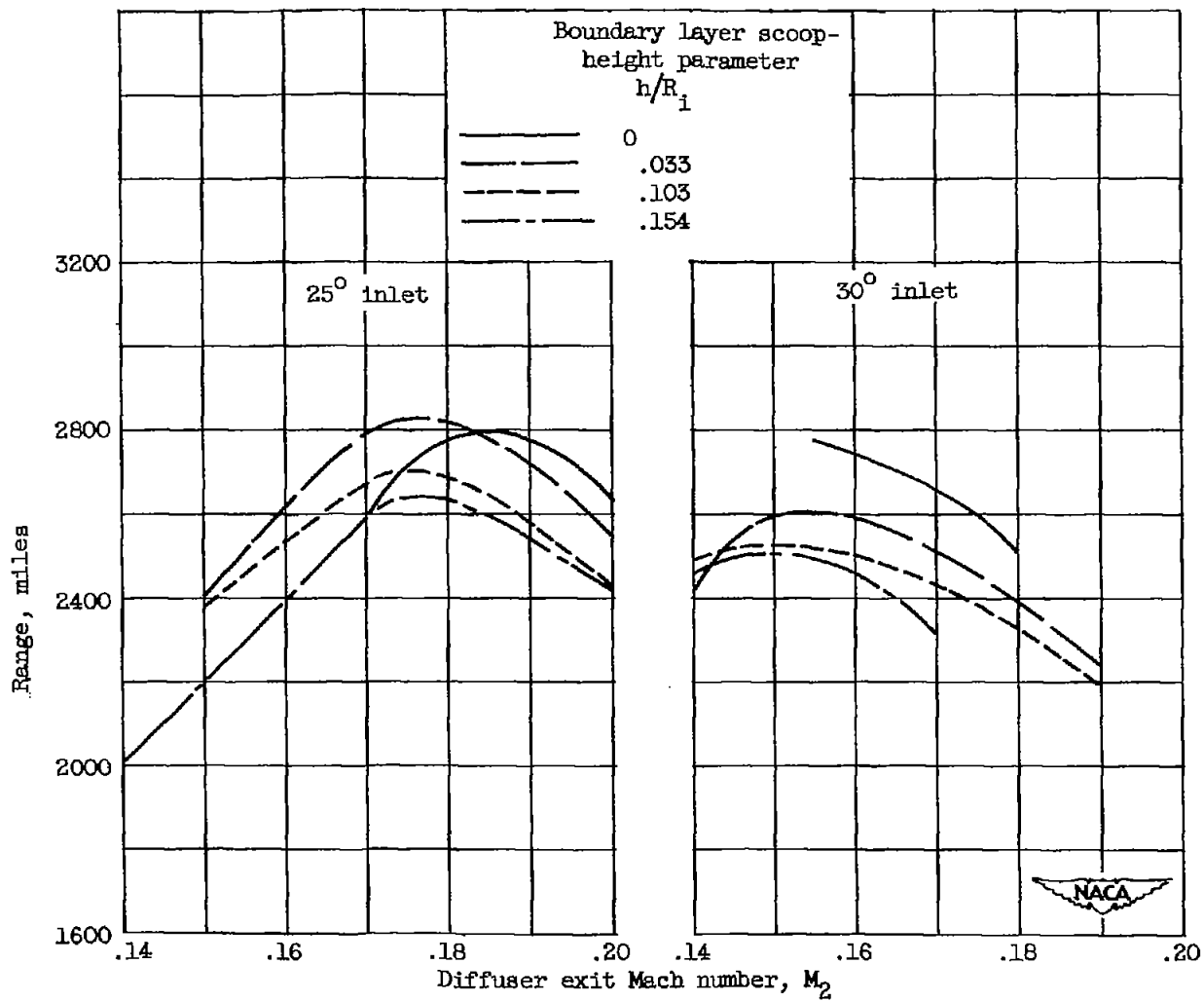


Figure 8. - Variation of range with diffuser exit Mach number for model 3 with 25° and 30° inlets and several boundary layer scoop heights. Free-stream Mach number, 2.0; altitude, 50,000 feet.

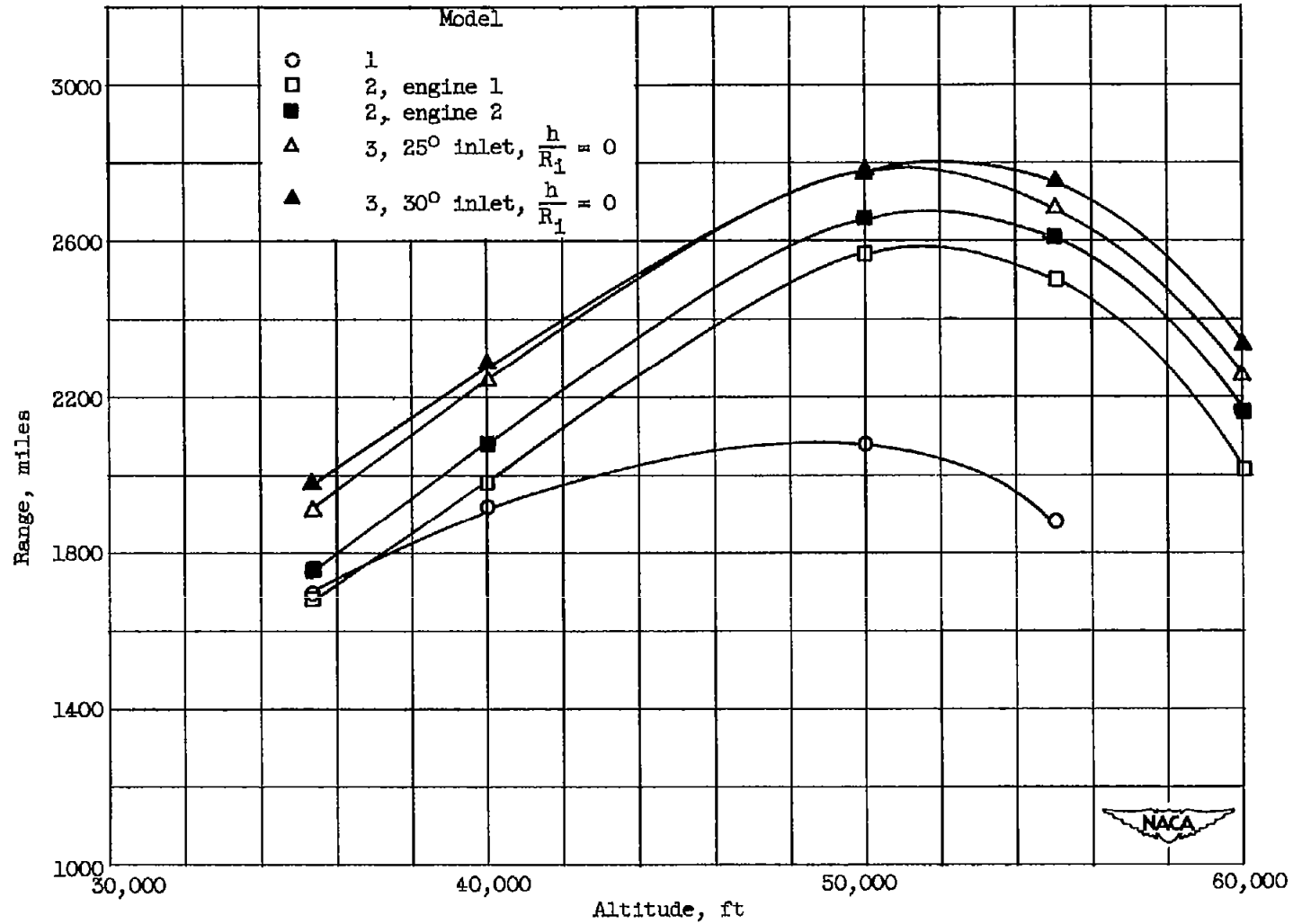


Figure 9. - Variation of maximum range with altitude for three models at free-stream Mach number of 2.0.

Model 1

Model 2

Model 3

Engine 1 Engine 2

25° inlet

30° inlet

$$\frac{h}{R_1} = 0$$

$$\frac{h}{R_1} = 0.154$$

$$\frac{h}{R_1} = 0$$

$$\frac{h}{R_1} = 0.154$$

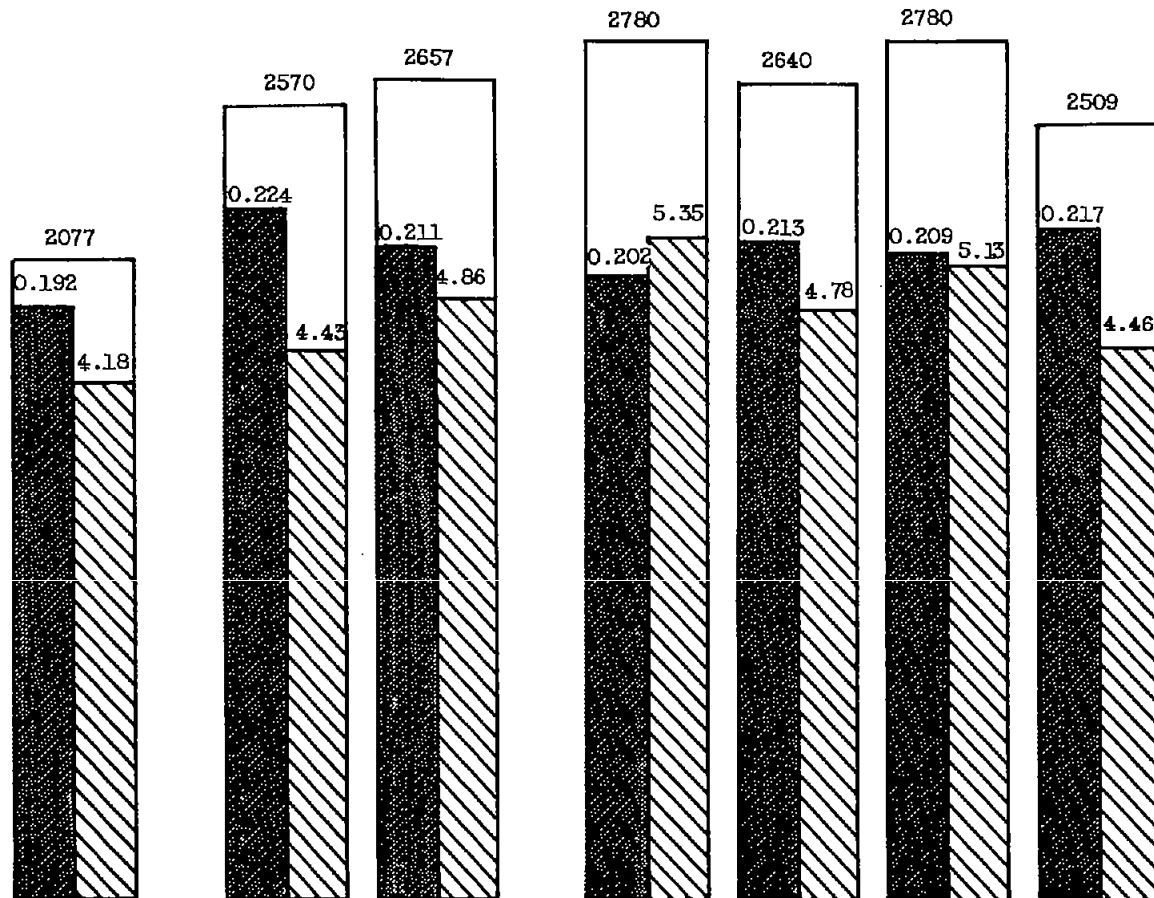


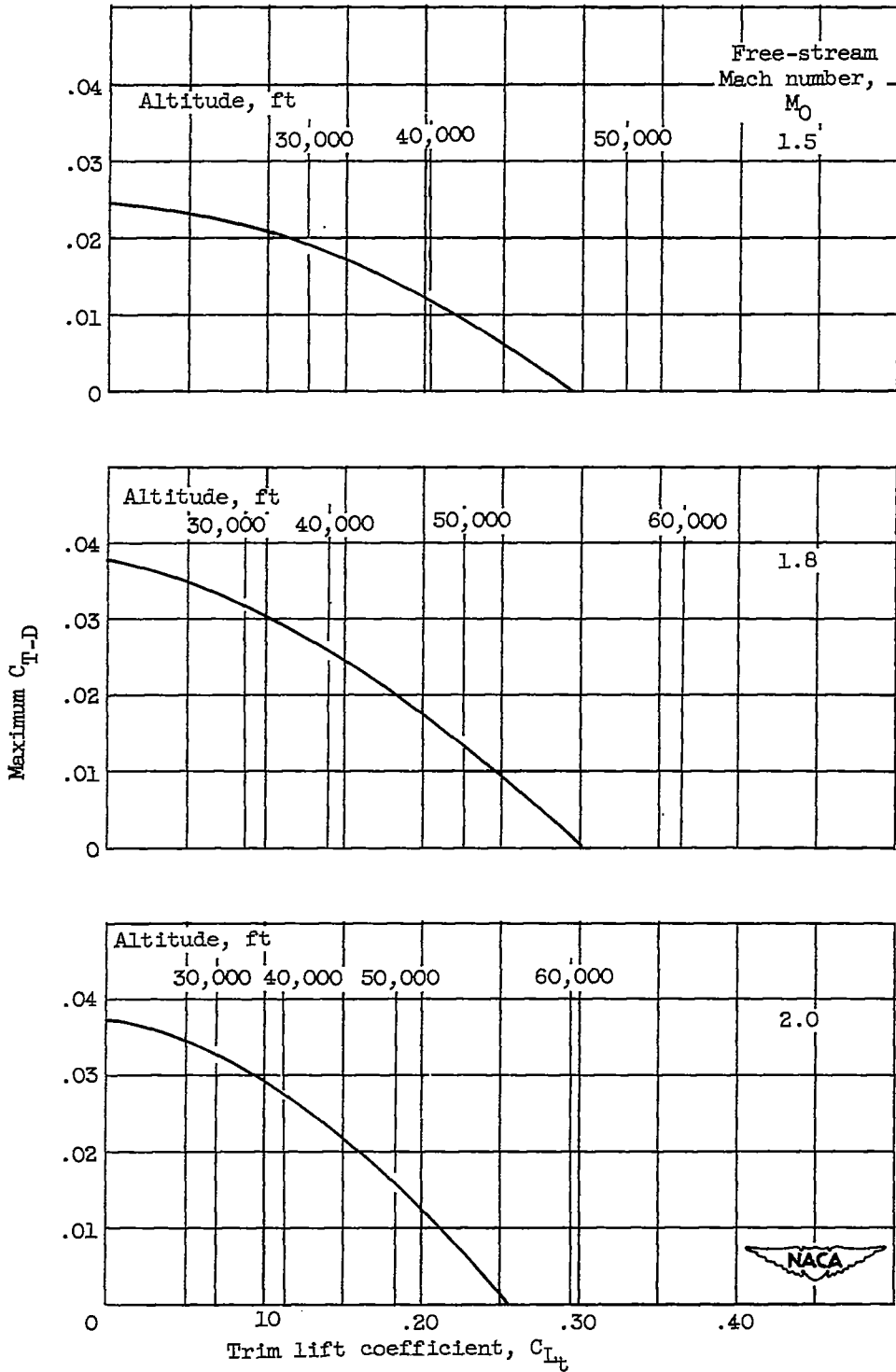
Figure 10. - Maximum range breakdown for three models at free-stream Mach number of 2.0 and altitude of 50,000 feet.

CONFIDENTIAL

CONFIDENTIAL

~~CONFIDENTIAL~~

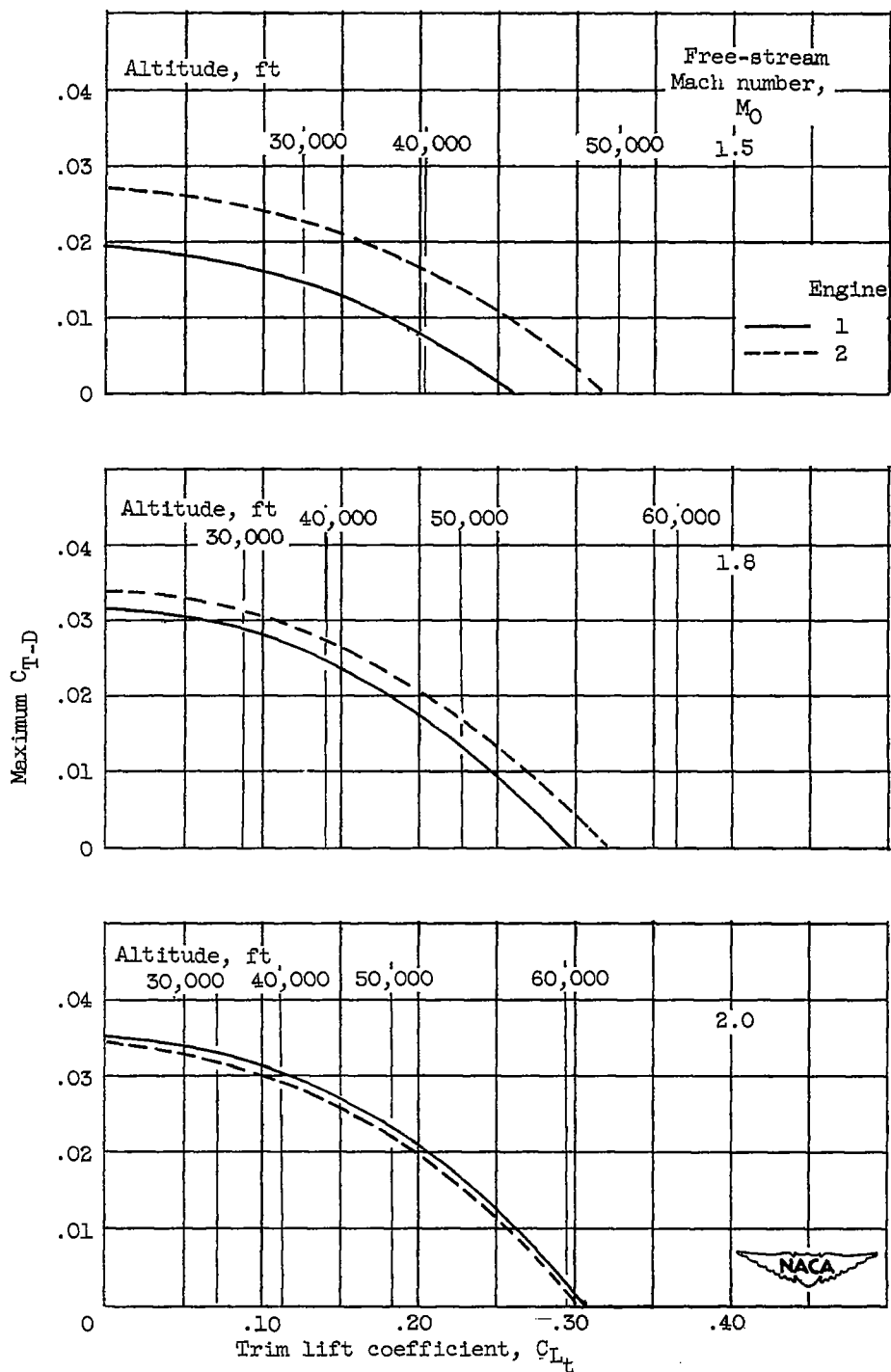
2931



(a) Model 1.

Figure 11. - Maximum coefficient of thrust minus drag as a function of trim lift coefficient at three free-stream Mach numbers.

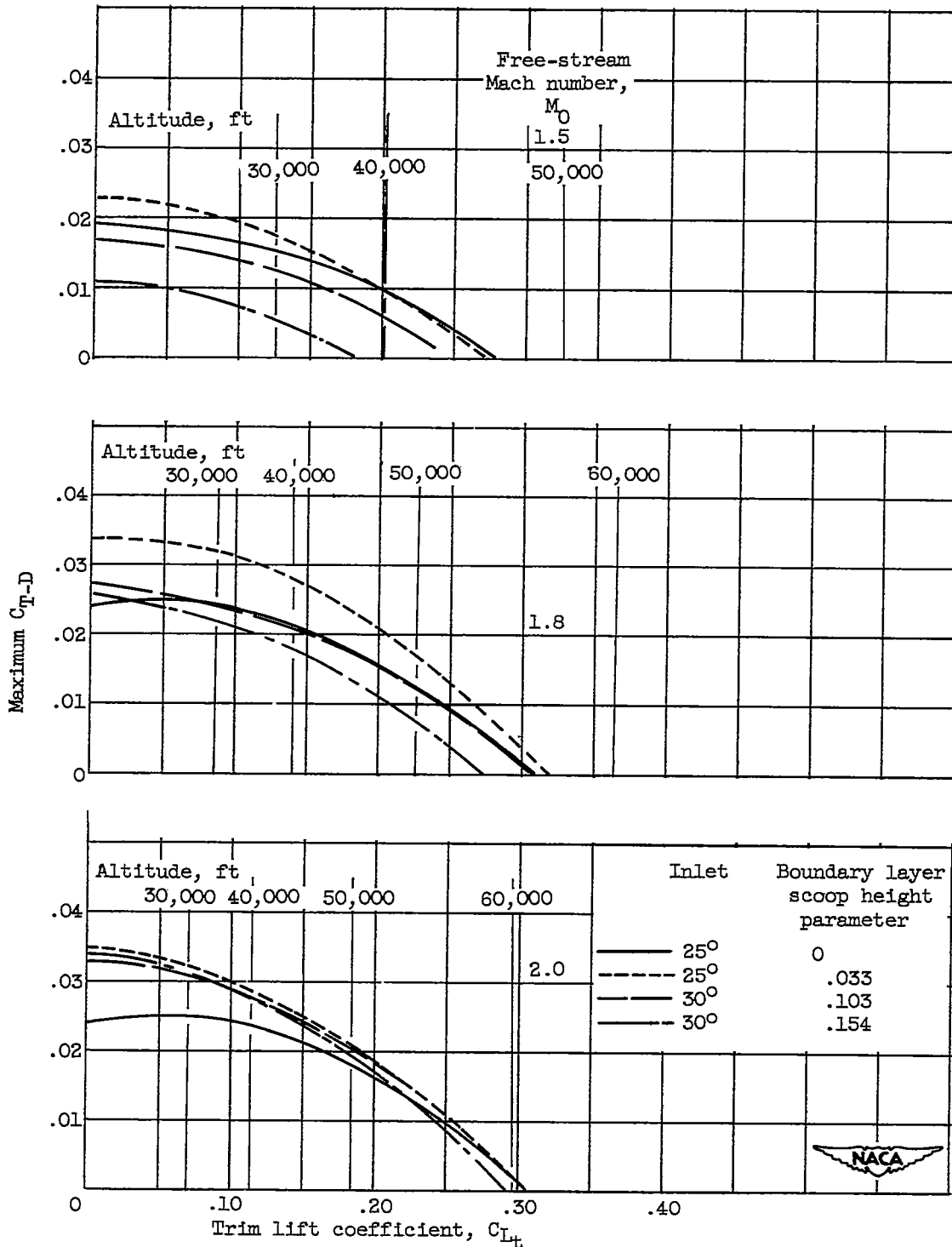
~~CONFIDENTIAL~~



(b) Model 2.

Figure 11. - Continued. Maximum coefficient of thrust minus drag as a function of trim lift coefficient at three free-stream Mach numbers.

2931



(c) Model 3.

Figure 11. - Concluded. Maximum coefficient of thrust minus drag as a function of trim lift coefficient at three free-stream Mach numbers.